Hindawi
Shock and Vibration
Volume 2019, Article ID 2586452, 13 pages
https://doi.org/10.1155/2019/2586452

Research Article

Seismic Analysis of Low-Rise Self-Centering Prestressed Concrete Frames considering Soil-Structure Interaction

Liang-Long Song,[1] **Tong Guo**,[2] **and Xin Shi**[2]

[1]*College of Civil and Transportation Engineering, Hohai University, Nanjing 210098, China*
[2]*School of Civil Engineering, Southeast University, Nanjing 210096, China*

Correspondence should be addressed to Liang-Long Song; songll@hhu.edu.cn

Received 27 August 2019; Accepted 22 November 2019; Published 11 December 2019

Academic Editor: Francesco Franco

In this study, the seismic behavior of low-rise self-centering (SC) prestressed concrete frames considering soil-structure interaction (SSI) is presented. For this purpose, a typical 4-story SC concrete frame, with and without flexible foundations, is analyzed through nonlinear dynamic analysis. Ground motion sets with two hazard levels are selected for analysis. A conventional reinforced concrete (RC) frame is also studied, and the structural demands of the RC and SC frames are compared in terms of peak and residual drifts, base shear, residual settlement, and rotation of foundation. The analysis results show that considering soil-structure interaction generally increases the peak and residual drift demands and reduces the base shear and connection rotation demands when compared to fixed base conditions. For the cases with and without flexible foundations, the SC frame is found to have comparable peak story drifts with the RC frame and have the inherent potential of significantly reducing the residual drifts. The seismic analysis results of the frames with flexible bases show that the RC and SC frames can experience foundation damage due to excessive residual foundation rotations after the maximum considered earthquake (MCE).

1. Introduction

Among various natural hazards, earthquakes represent one of the most devastating disasters which can induce overwhelming damage to civil infrastructure. Recent catastrophic earthquakes have highlighted the limitations of traditional building code provisions, in which the structural elements of seismic resistant systems are expected to yield and then dissipate energy under strong earthquakes. Based on this energy dissipation mechanism, it is reasonable to expect significant residual deformation and distributed structural damage in the conventional seismic structural systems after a strong earthquake. The field surveys after recent seismic events showed that many seismically damaged building structures had to be demolished due to unacceptable repair costs, even though they did not experience severe structural damage or collapse [1, 2].

Concerns about the issues associated with the conventional earthquake-resistant structural systems have led to the development of many innovative earthquake-resistant structural systems with higher performance levels. Over the past several decades, numerous studies have been made to develop a variety of self-centering (SC) earthquake-resistant systems in which the structural damage and residual deformation following an earthquake is minimized [3–10]. Among the different self-centering systems, self-centering concrete frames can be used as alternatives to conventional reinforced concrete (RC) frames. The early versions of SC concrete frames use unbonded PT steel to connect the precast beam and column and provide the self-centering capability [11], and the gap opening/closing behavior is allowed at the interface between the beam and column. To mitigate the seismically induced displacement demands, early research efforts increase the energy-dissipation capacity of SC concrete frames by using yielding devices [12–14] in SC beam-column connections. However, yielding devices can be damaged or are not easy to be replaced after strong earthquakes. Therefore, Morgen and Kurama [15]

developed easily replaceable friction devices which are located at the top and bottom surfaces of beam ends. Song et al. [16, 17] proposed a novel SC concrete frame, which uses unbonded PT tendons to provide self-centering capability and bolted web friction devices (WFDs) to dissipate energy in earthquakes. These WFDs are installed at the beam webs and thus cause no any interference with the floor slab, as compared with the SC beam-column connections in Morgen and Kurama [15]. In addition, steel jackets are used at the beam ends to protect the concrete at the beam-column interfaces from damage.

Several research efforts have numerically evaluated the nonlinear behavior of self-centering concrete moment frames. Cheok et al. [18] performed a parametric investigation on the seismic response of hybrid precast unbonded post-tensioned (UPT) concrete frames [12] and concluded that the hybrid frames can have a comparable or better performance than the conventional monolithic cast-in-place RC frames. Similar conclusion was drawn by Morgen and Kurama [19] through a comparative assessment of the UPT frames with friction-damped systems and the conventional RC frames. More recently, Song et al. [20] studied the behavior of SC concrete frames with web friction devices (WFDs), and both the structural and member seismic demands were evaluated.

It is worth noting that past studies on self-centering frames were performed assuming a rigid foundation, and usually the soil flexibility beneath the frame structure is not considered. Despite the fact that soil-structure interaction (SSI) has significant influence on the seismic responses of structures [21–25], little investigation is performed to study the effect of SSI on self-centering concrete frames. Therefore, taking a low-rise 4-story frame building as an example, this paper analytically investigates the seismic behavior of self-centering concrete frames with the consideration of SSI. A SC frame and a conventional RC frame (both with a fixed-base and a flexible-base) are designed and comparatively assessed through nonlinear dynamic analyses under three hazard levels of earthquake ground motions.

2. Self-Centering Concrete Frame with Web Friction Devices (WFDs)

A typical SC concrete frame with web friction devices (WFDs) [16] is illustrated in Figure 1, where the precast concrete beams are connected to columns using horizontally-oriented unbonded PT tendons, which provide the self-centering capability of the frame under seismic loading. Steel jackets are shop fabricated at the ends of beam, and the column faces are armed with steel plates, to prevent the concrete from damage at the interfaces of beam and column. WFDs are used at the beam ends to dissipate seismic energy when the connection gap opens and closes. A WFD consists of two steel channels (Figure 1(b)) bolted to the column through the steel connection plates and high-strength bolts. The webs of steel channels are adhered with brass friction plates and are compressed to the steel jacket using friction bolts, which can provide normal forces on the friction surfaces. Circular holes in the steel jacket and beam shown in Figure 1(b) can accommodate the motion of friction bolts during gap opening/closing of the beam-column connection.

3. Design of the Frame-Foundation System

A prototype RC frame for a 4-story, 3×3-bay building located in Los Angeles, California, is selected for analysis as the basis to design the SC frame. The prototype RC frame is designed by Haselton and Deierlein [26] as a ductile frame in accordance with ICC-2003 [27], ASCE 7-02 [28], and ACI 318-02 [29] and is assumed to be in a stiff soil site. The seismic design of the ductile RC frame is based on the mapped hazard using $S_s = 1.5\,\mathrm{g}$ and $S_1 = 0.6\,\mathrm{g}$ (g is the acceleration of gravity). Figure 2(a) shows the plan view of the prototype building. It is seen that the lateral load resisting systems of the prototype structure consists of four identical frames in each primary direction. This study examines the seismic response of one of the interior frames, as shown in the elevation view of the frame (Figure 2(b)). The story heights of the first story and other stories of the frame are 4.6 m and 4.0 m, respectively. The design dead load is $8.38\,\mathrm{kN/m^2}$, while the design live load is $2.39\,\mathrm{kN/m^2}$. Table 1 summarizes the major design parameters of the RC frame.

To facilitate a comparative assessment, the beam/column section dimensions and reinforcement details of column members of the SC frame are assumed to be identical to those of the prototype RC frame. The reinforcement ratios of beams in the SC frame are set to be 0.5%, according to the suggestion by Song et al. [16]. The connection design M_{IGO} is assumed to be the mean value of positive and negative flexural strength at the RC frame beam ends. M_{IGO} is contributed by the moment due to the initial PT force resultant in the beam M_{T0} and the moment due to the friction force resultant in the WFD, M_{Ff}, is as follows:

$$M_{\mathrm{IGO}} = M_{\mathrm{T0}} + M_{\mathrm{Ff}} = T_0 \cdot d_0 + F_{\mathrm{f}} \cdot r, \tag{1}$$

where T_0 and F_{f} represent the initial PT force resultant and the friction force resultant, respectively. d_0 is the distance from the connection rotation point to the beam section centroid, and r is the distance from the connection rotation point to the friction force resultant. The values of T_0 and F_{f} can be determined according to equation (1) and the connection's hysteretic energy dissipation ratio, β_E, can be expressed as follows:

$$\beta_E = \frac{M_{\mathrm{Ff}}}{M_{\mathrm{IGO}}}. \tag{2}$$

In this study, $\beta_E = 0.48$ is used in equation (2). Table 1 also summarizes the design parameters of the SC concrete frame, such as the initial PT force resultant, T_0, the friction force resultant in the WFD, F_{f}, and the cross-sectional area of PT tendons, A_p, which can be calculated using T0 and f_{pi}, where $f_{pi} = 0.50 f_{py}$ = the design initial stress of PT tendons and $f_{py} = 1675$ MPa = the design yield strength of PT tendons.

In this study, four cases are considered, including the RC frame with fixed bases (RC-FB) and flexible foundations (RC-SSI), along with the SC frames with fixed bases (SC-FB)

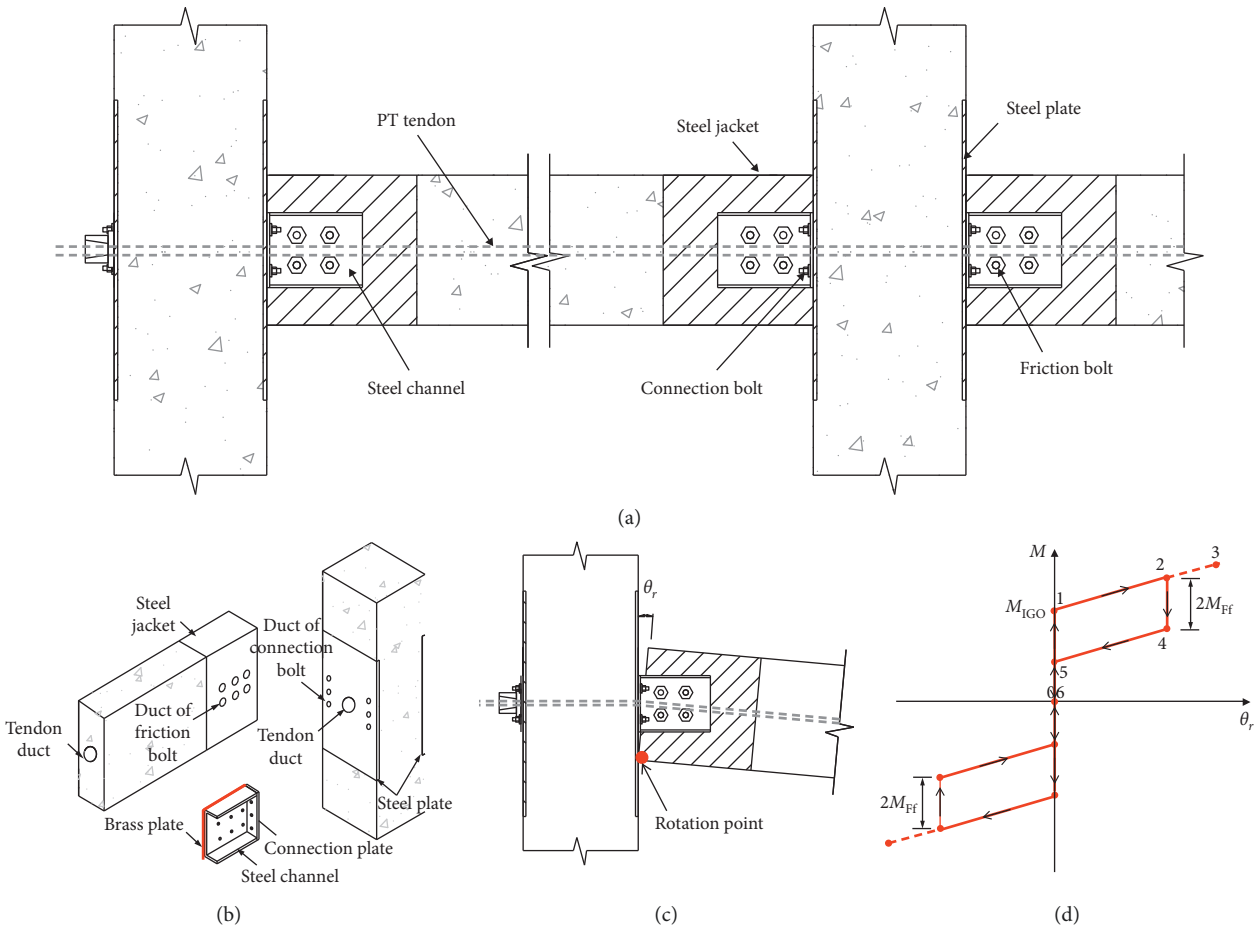

Figure 1: SC concrete frame with web friction devices. (a) Profile of the SC frame. (b) Configuration of beam-column connection. (c) Gap-opening behavior. (d) Conceptual $M-\theta_r$ behavior.

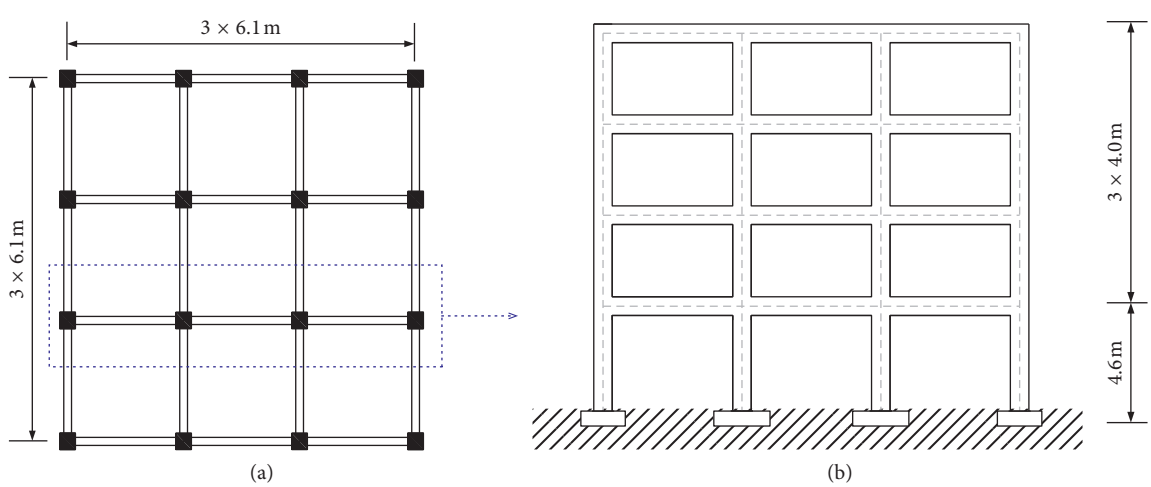

Figure 2: Plan and elevation views of the prototype building. (a) Plan view. (b) Elevation view.

and flexible foundations (SC-SSI). As shown in Figure 2(b), square isolated footings are designed for the foundation systems of the RC and SC frames. The footings are assumed to be rested on dense silty sand at the prototype building site and the soil properties are unit weight $\gamma = 18\,\text{kN/m}^3$, friction angle $\phi = 18^\circ$, while cohesion $c = 5\,\text{kPa}$. The foundations are designed according to the bearing capacity theory of Meyerhof [30], and the vertical safety factor is assumed to be 3. As a result, the internal footings are designed as $1.9\,\text{m} \times 1.9\,\text{m} \times 0.5\,\text{m}$, and external footings are designed as $1.5\,\text{m} \times 1.5\,\text{m} \times 0.5\,\text{m}$, while the embedment depth is 0.5 m for both the internal and external footings.

Table 1: Design characteristics of the RC and SC frames.

Floor	Column size (mm × mm)		Column total reinforcement ratio (%)		Beam size (mm × mm)	RC beam reinforcement ratio (%)		T_0 (kN)	F_f (kN)	A_p (mm^2)
	Exterior	Interior	Exterior	Interior		Bottom	Top			
1	558 × 558	558 × 558	1.30	1.63	609 × 558	0.43	0.83	890	821	1112
2	558 × 558	558 × 558	1.30	1.63	609 × 558	0.37	0.75	815	752	973
3	558 × 558	558 × 558	1.13	1.45	609 × 558	0.32	0.60	696	642	834
4	558 × 558	558 × 558	1.13	1.45	609 × 558	0.32	0.45	609	563	695

4. Analytical Models

4.1. Modeling of RC and SC Frames. The 2D numerical models of the RC and SC frames are constructed using the open-source software OpenSees [31] to perform the modal and nonlinear dynamic analyses. For the RC frame, each beam is modeled using a linear elastic beam-column element (elasticBeamColumn element in OpenSees) with a lumped plasticity hinge element (zeroLength rotational element in OpenSees) at either end of the beam. The lumped plasticity hinge element was developed by Ibarra et al. [32] and incorporates a hysteretic model defined by a trilinear backbone curve and associated hysteretic rules, which can consider the strength and stiffness deterioration. The modeling parameters of the lumped plasticity hinge element were calibrated to the experimental results of RC beams with ductile detailing [33] and have been used by several researchers for the performance evaluation of ductile RC frames [34, 35]. According to Haselton and Deierlein [26], an elastic zeroLength rotational element is used to model the panel zone shear deformations of the RC frame. Due to the existence of axial loads in the column, the column is modeled using the force-based nonlinear beam-column element (forceBeamColumn element in OpenSees), which can consider the interaction of axial load-flexural bending moment. The forceBeamColumn element can also capture the distributed plasticity with fiber-sections at the integration points along the element. These fiber-sections represent the cross sections of the structural members and are composed of a number of meshed fibers. Each fiber is assigned with a uniaxial stress-strain relationship of a particular material, such as concrete and steel reinforcement. The force-deformation relationship of the fiber section is determined by the integration of the stress-strain relationship over the section. In this study, steel reinforcement is modeled using the uniaxial Giuffré–Menegotto–Pinto model (Steel02 material in OpenSees), while concrete is simulated through the uniaxial Kent–Scott–Park model (Concrete01 material in OpenSees) [36].

The analytical model for the SC frame with WFDs is constructed using the SC beam-column connection model proposed by Song et al. [16] (Figure 3(a)). The beam and column members of the SC frame are simulated using the forceBeamColumn elements in OpenSees. The interface between the beam and column is modeled using pairs of rigid elasticbeamcolumn elements, which are based on the elasticbeamcolumn element in OpenSees with very large axial and bending stiffness. To model the connection gap opening and closing behavior, two zeroLength contact elements with compression-only behavior are used at the top and bottom rotation points, as seen in Figure 3(a). The steel channel is modeled using the elasticbeamcolumn element in OpenSees. One end of the channel element is connected to the side node of panel zone, and the other node is connected to the beam element node using a zeroLength Section element in OpenSees, which is incorporated with bidirectional plasticity properties and used to simulate the friction force resultant in the steel channel. The beam-column panel zone is modeled using eight rigid elasticbeamcolumn elements representing the boundaries of the panel zone, and a zeroLength rotational element with bilinear elastic moment-rotation relationship is used to simulate the panel zone shear deformation. In addition, the PT tendon is modeled using a truss element with an initial strain. The comparison of the SC beam-column connection moment versus relative rotation relationship of the experiment and numerical simulation is shown in Figure 3(b). Further details of the SC connection model can be found in [16].

4.2. Modeling of SSI. The soil-structure system of the frame is simulated using the Beam on Nonlinear Winkler Foundation (BNWF) model [37] (Figure 4(a)), which includes a series of zeroLength elements of vertical direction (*q-z* springs) beneath the foundation, and two zeroLength elements of horizontal direction (*p-x* and *t-x* springs). The zeroLength *q-z* springs are used to simulate the vertical and rocking behavior of the foundation. The zeroLength *p-x* and *t-x* spring elements are used to simulate the lateral passive soil behavior and the friction behavior beneath the foundation, respectively. As seen in Figure 4(b), the force-displacement relationship of the *q-z* spring is defined using the QzSimple2 uniaxial material in OpenSees, which exhibits an asymmetric hysteresis behavior with a large compressive capacity and a small tensile capacity (5% of compressive capacity), considering the small tension strength of soil. The PxSimple1 uniaxial material with a pinching hysteresis response (Figure 4(c)) is assigned to the *p-x* spring element to consider the potential gaping of embedded shallow footing under seismic loading. As seen in Figure 4(d), the TxSimple1 uniaxial material is used to define the constitutive relationship of the *t-x* spring element to account for the frictional behavior when the foundation slides. The above three uniaxial material models for the zeroLength spring elements were originally proposed by Boulanger et al. [38] and later validated to experimental results of shallow foundations by Raychowdhury and Hutchinson [39].

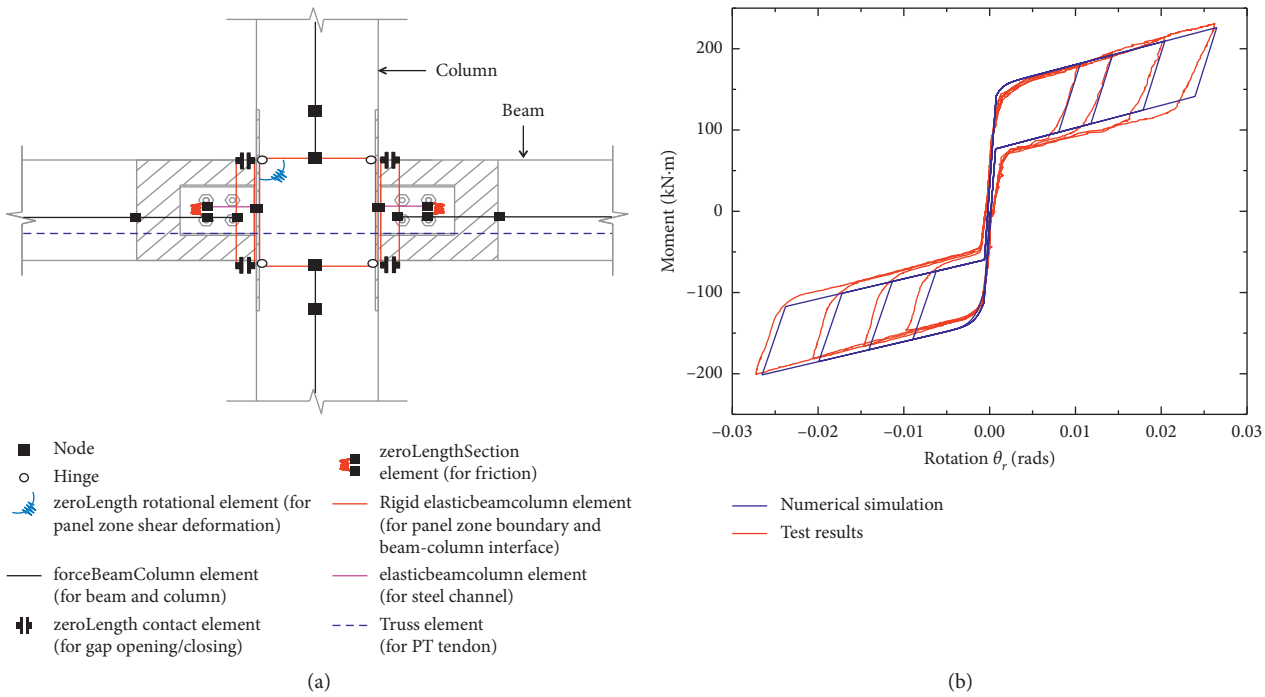

Figure 3: Numerical model for the SC beam-column connection and experimental validation. (a) OpenSees model of SC beam-column connection. (b) Comparison of numerical and experimental results [16].

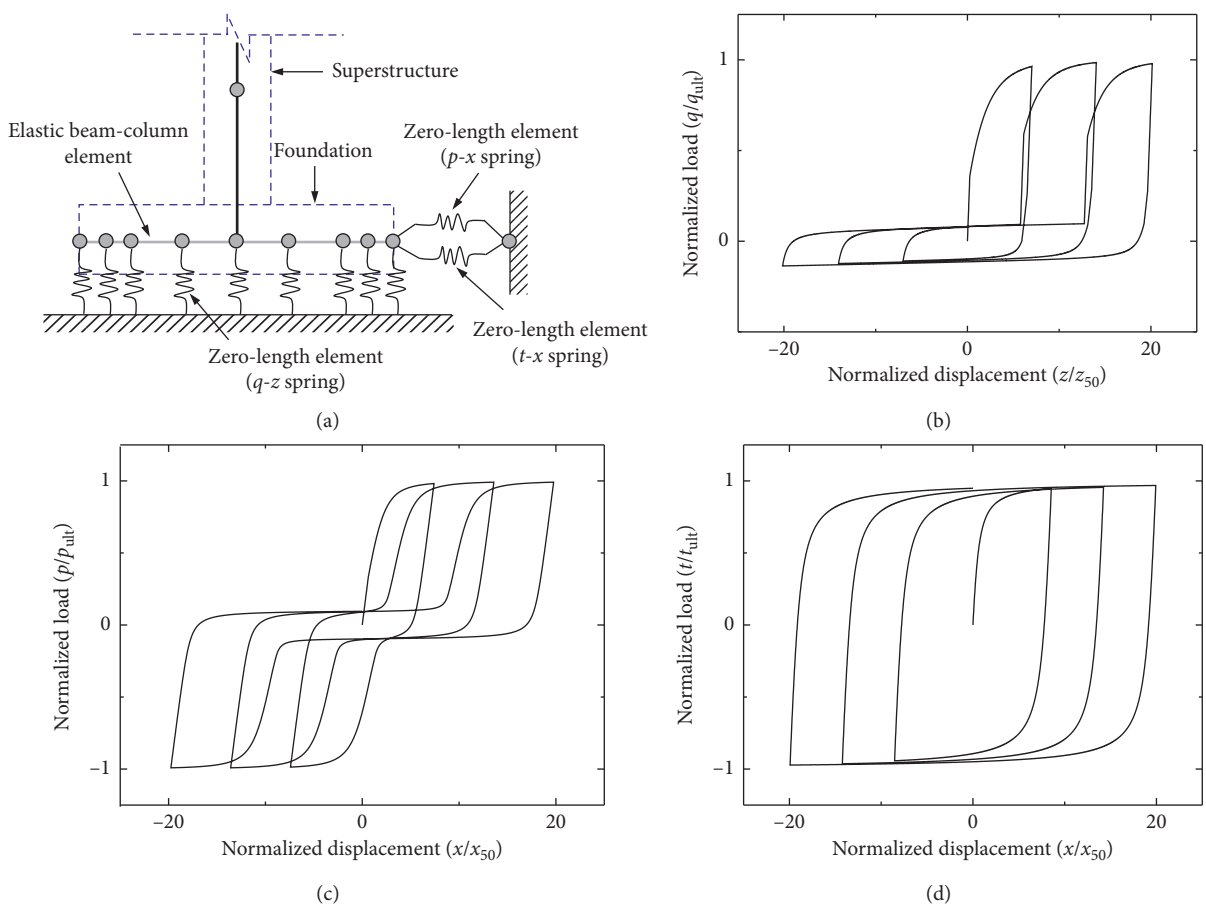

Figure 4: The BNWF model and behavior of soil spring for the foundation. (a) The BNWF model. Behavior of (b) q-z model, (c) p-x model, and (d) t-x model.

To achieve desirable rocking stiffness, the vertical springs beneath the footing are not equally spaced in the BNWF model. In accordance with the suggestions in Harden and Hutchinson [37] and ATC-40 [40], the vertical spring spacing at the middle segment (80% of the footing length) is assumed to be 2% of the footing length, while the spacing at the two end segments is assumed as 1% of the footing length. The stiffness intensity of the end segment is five times that of the middle segment.

According to the results of modal analysis, the first vibration periods of the RC-FB and SC-FB frames are 0.630 s and 0.629 s, respectively. When the SSI is considered, the first vibration periods are increased to 0.738 s and 0.742 s for the RC-SSI and SC-SSI frames, respectively, indicating the period elongation effect of SSI. The nonlinear dynamic analyses of the RC and SC frames are performed with a Rayleigh damping ratio of 5% for the first and third vibration modes. Every analysis is conducted using an actual earthquake record and an additional zero acceleration time-history (20 s) to calculate the residual displacements accurately.

5. Earthquake Ground Motions

A set of ten earthquake records (Table 2) is used for the nonlinear dynamic analysis. These earthquake records are all far-fault ground motions recorded at stiff soil sites and are scaled to the hazard levels of design-based earthquake (DBE) and the maximum considered earthquake (MCE), respectively. Figure 5(a) shows the 5% damped mean (m) response spectrum of the scaled ground motions and ASCE 7-02 DBE design spectrum [28], as well as the one standard deviation (σ) spectra of the ground motions. Figure 5(b) compares the DBE design spectra and the individual earthquake spectra scaled to DBE. It can be seen that the mean spectrum of the selected earthquake records matches the DBE design response spectrum very well.

6. Seismic Performance Evaluation

Figure 6 shows the roof drift time histories of the RC and SC frames with different base conditions under the LP89slc record scaled to DBE and MCE. It is seen that, for both cases of fixed-base and flexible-base, the maximum roof drifts of the RC and SC frames are similar at the DBE and MCE.

For example, when subjected to DBE-level LP89slc record, the maximum roof drifts of the RC-FB and SC-FB frames are 0.872% and 0.871%, respectively, and the maximum roof drifts of the RC-SSI and SC-SSI frames are 1.30% and 1.20%, respectively. In addition, the peak roof drifts of structures with flexible bases (i.e., RC-SSI and SC-SSI frames) are higher than those of fixed base structures (i.e., RC-FB and SC-FB frames). The residual roof drifts are smaller for the SC frames compared with the RC frames, especially for the cases with flexible foundations. When the soil-structure interaction (SSI) is considered, the residual roof drift of the RC frame experiences a significant increase. However, the incremental effect of SSI on the residual drift of the SC frame is much less. For example, under the DBE-level LP89slc record, the residual roof drift ratios of the RC-FB and RC-SSI frames are 0.07% and 0.26%, respectively, and are 0.05% and 0.07% for the SC-FB and SC-SSI frames, respectively, as can be seen in Figures 6(a) and 6(b). Similar observations can be seen for the residual roof drift ratios of RC and SC frames under the MCE-level LP89slc record, as shown in Figures 6(c) and 6(d).

To study the effect of soil-structure interaction (SSI) on the local behavior of SC frames, the beam end moment-relative rotation ($M - \theta_r$) responses of the connection located at the left of Bay 1, Floor 3 of the SC-FB and SC-SSI frames are shown in Figure 7. The local connection responses shown in Figure 7 are obtained under the LP89slc record scaled to DBE and MCE. It is found that the connection of the SC-SSI frame experiences less rotation and thus dissipates less earthquake energy than the connection of the SC-FB frame. For example, under the DBE-level LP89slc ground motion, the maximum rotation and dissipated energy for the connection of the SC-FB frame are 0.0046 rad and 4.6 kN·m, respectively, while the values for the connection of the SC-SSI frame are 0.0025 rad and 2.0 kN·m, respectively. This phenomenon can be explained that when the soil-structure interaction (SSI) is considered, the foundations of the SC frame would experience rotational and sliding deformations, and thus the deformation demands of the superstructure are reduced. Similar observation can be made under the MCE-level LP89slc ground motion, as shown in Figure 7(b).

Figure 8 illustrates the distribution of average values of peak story drifts over the height of each structure under the DBE- and MCE-level records. It is found that the peak story drift is at the first floor in all cases. The largest values of peak story drifts of the RC-FB frame under the DBE- and MCE-level records are 1.28% and 2.25%, respectively, while the values of the SC-FB frame are slightly larger, i.e., 1.44% and 2.50%, respectively. Compared to the RC-FB frame, the largest values of peak story drifts of the RC-SSI frame are increased by 67.19% and 60% under the DBE- and MCE-level excitations, respectively; and the increases for the SC-SSI frame are 36.81% and 37.6%, respectively. In addition, it is seen that the largest values of peak story drifts of the RC-SSI frame are slightly larger than those of the SC-SSI frame under DBE- and MCE-level excitations.

Figure 9 plots the distribution of average values of residual story drifts over the building height. The largest values of residual story drifts of the RC and SC frames increase when the SSI is considered, and the largest residual story drift is at the first story in all cases, which are similar to the trends in Figure 8. Under both the DBE- and MCE-level excitations, the RC-SSI and SC-SSI frames produce nearly uniform residual story drifts at the second to fourth floors. When subjected to the DBE and MCE-level excitations, the RC-FB and RC-SSI frames experience nonnegligible residual drifts in most stories. The largest values of residual story drift ratios for the RC-FB and RC-SSI frames are 0.18% and 0.26%, respectively, under the DBEs, and are 0.45% and 0.61%, respectively, under the MCEs. Compared to the RC frames, the SC frames (with and without flexible base conditions) experience significantly lower residual story drifts. The largest residual story drifts of the SC-FB and SC-

Table 2: Characteristics of the selected earthquake records.

ID	Earthquake	Station	Record	Scale factor	
				DBE	MCE
1	Imperial valley, 1979	Cucapah	IV79qkp	1.75	2.62
2	Loma Prieta, 1989	Gilroy array #4	LP89g04	1.37	2.05
3	Loma Prieta, 1989	Hollister City Hall	LP89hch	1.54	2.31
4	Loma Prieta, 1989	Hollister differential array	LP89hda	1.79	2.68
5	Northridge, 1994	Canoga Park-Topanga Can.	NR94cnp	0.94	1.40
6	Northridge, 1994	Northridge-17645 Saticoy St.	NR94stc	1.26	1.89
7	Superstition Hills, 1987	El Centro Imp. Co. Cent	SH87icc	1.65	2.47
8	Superstition Hills, 1987	Westmorland Fire Station	SH87wsm	2.46	3.69
9	Loma Prieta, 1989	Palo Alto—SLAC lab	LP89slc	1.78	2.66
10	Northridge, 1994	LA—Centinela St.	NR94cen	1.79	2.69

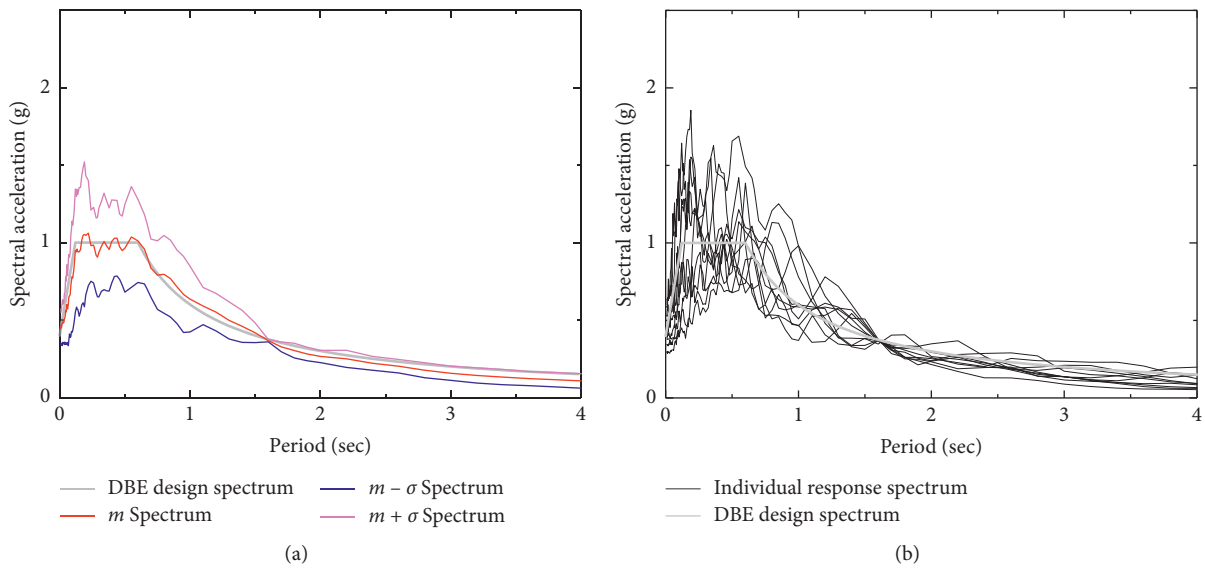

Figure 5: Comparison of the design spectrum with the spectra of the ground motions. (a) Mean and DBE spectra. (b) Individual spectra scaled to DBE.

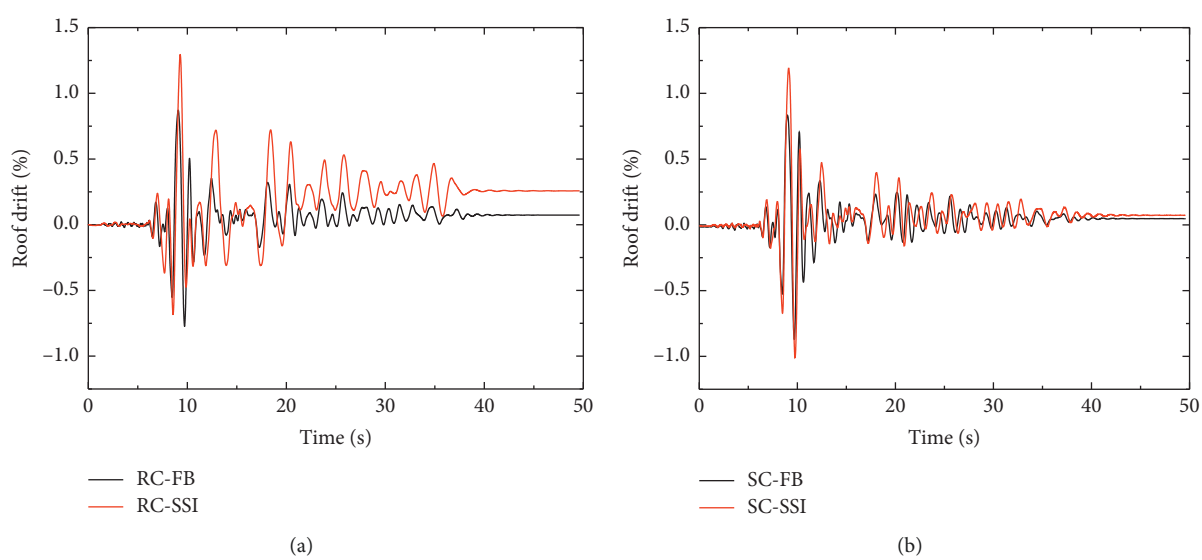

Figure 6: Continued.

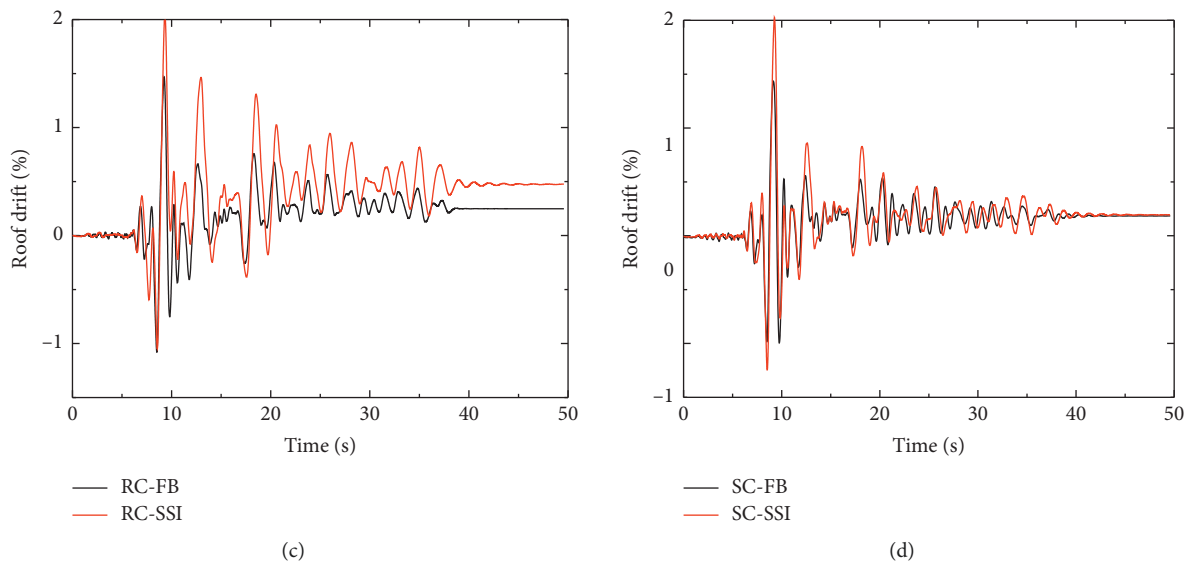

Figure 6: Roof drift-time histories under the LP89slc record scaled to DBE and MCE. (a) RC frames (DBE). (b) SC frames (DBE). (c) RC frames (MCE). (d) SC frames (MCE).

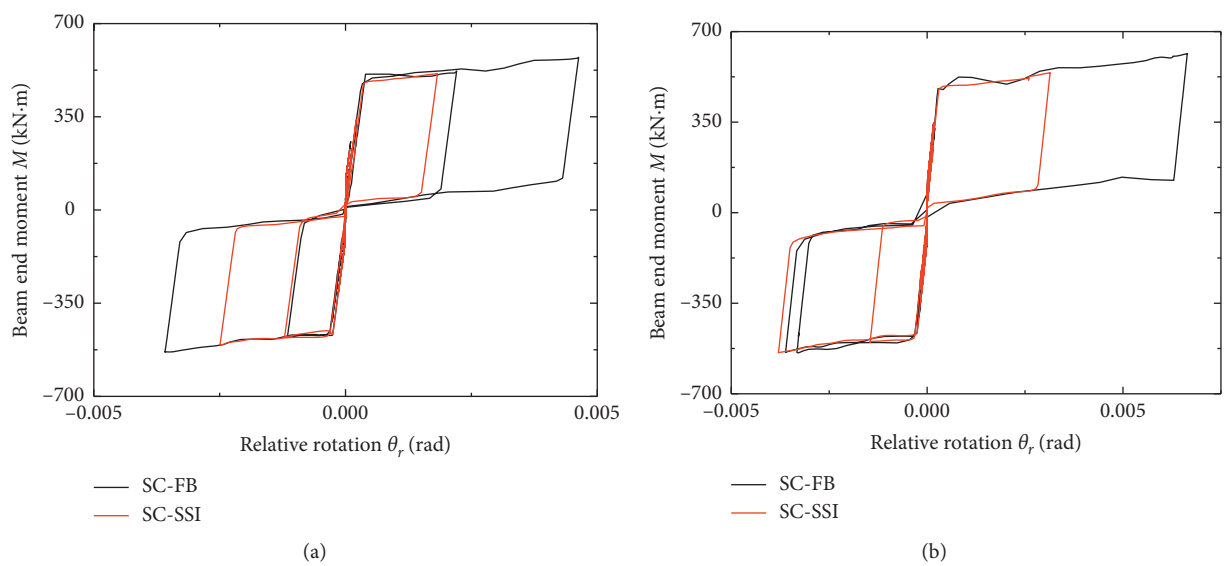

Figure 7: Connection behavior of the SC frames under the LP89slc record scaled to DBE and MCE. (a) DBE. (b) MCE.

SSI frames are 0.11% and 0.14%, respectively, under the DBEs, and they are 0.29% and 0.32%, respectively, under the MCEs.

Figure 10 plots the normalized base shear demand base shear of SSI model, V_{SSI}, divided by the base shear of fixed base model, V_{FB}) of theRC-SSI and SC-SSI frames. It is seen that SSI tends to lower the base shear demands, and the reduction of base shear of the RC-SSI frame is more pronounced than that of the SC-SSI frame. For the RC-SSI frame, the mean values of V_{SSI}/V_{FB} are decreased by 31.15% and 29.45% under the DBE-and MCE-level excitations, respectively; and they are 11.66% and 7.80% for the SC-SSI frame.

The nonlinear foundation behavior is evaluated using the residual foundation settlement and residual foundation rotation, which are considered as criteria of foundation damage. Table 3 presents the damage classification criteria of foundations summarized by Nakano et al. [41]. The residual settlements and rotations of foundation can be estimated using the BNWF model with reasonable accuracy, according to the model calibration using the experimental results [42]. Figure 11 shows the residual foundation settlements of the RC-SSI and SC-SSI frames under the DBE- and MCE-level excitations. It is seen that both the RC-SSI and SC-SSI frames experience no foundation damage due to residual foundation settlements, since the residual foundation settlements are all below 0.05 m, which is the limit value for none damage. Compared to the RC-SSI frame, the residual settlements of the SC-SSI frame are much lower in all cases. When subjected to the DBE- and MCE-level excitations, the

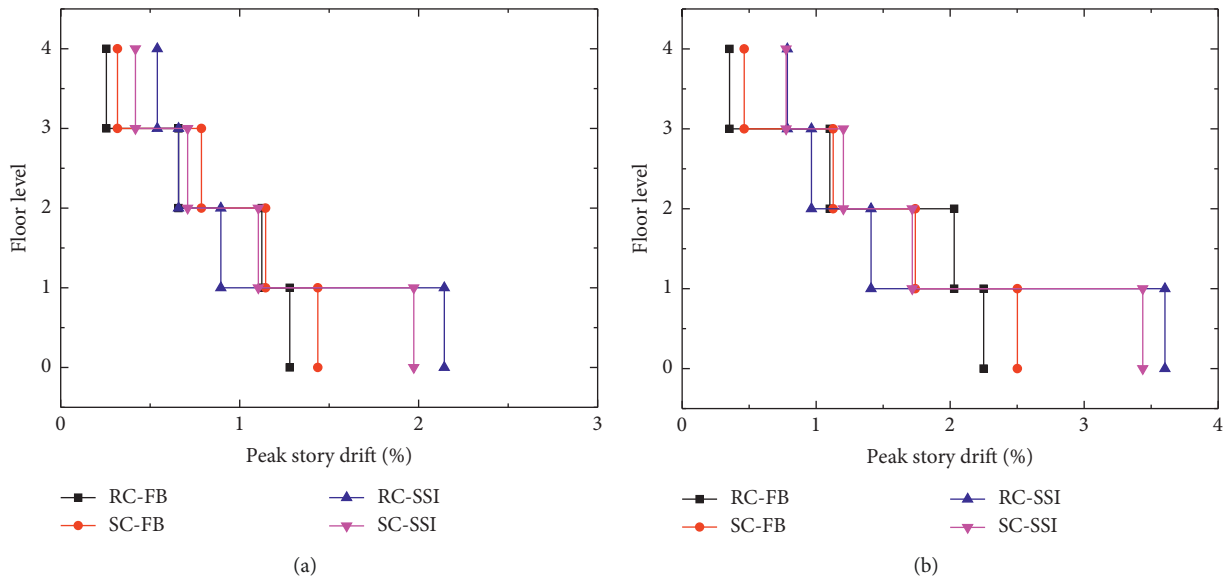

Figure 8: Peak story drift ratios of the RC and SC frames. (a) DBE. (b) MCE.

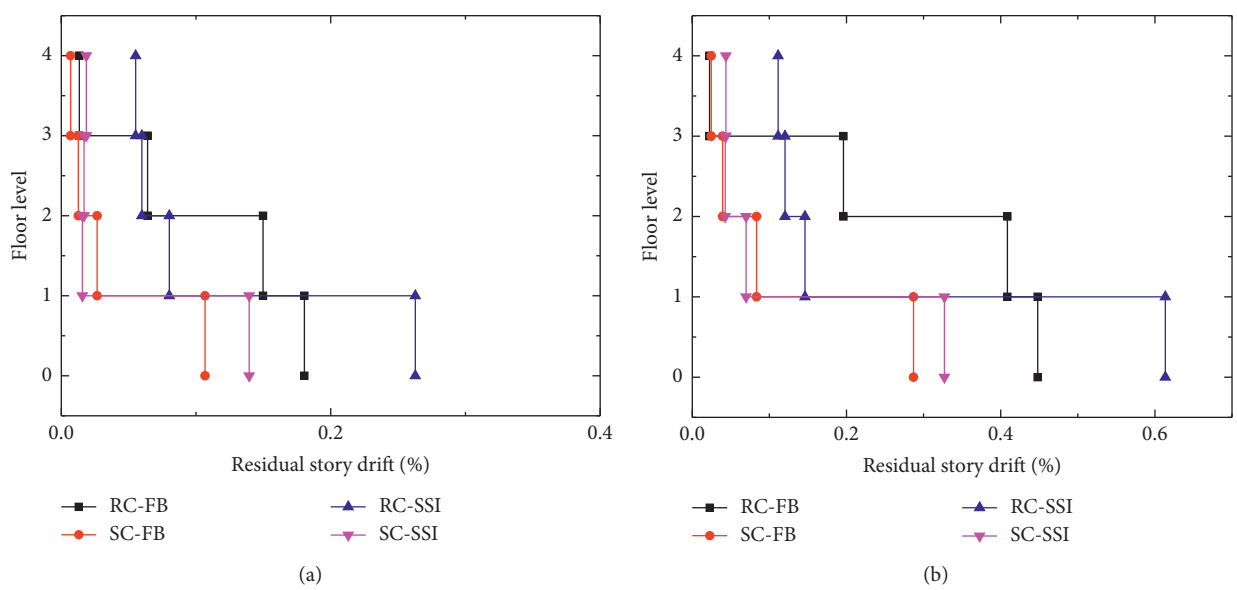

Figure 9: Residual story drift ratios of the RC and SC frames. (a) DBE. (b) MCE.

average residual settlements of the RC-SSI frame are 0.021 m and 0.032 m, respectively, whereas the average residual settlements of the SC-SSI frame are significantly lower, i.e., 0.005 m and 0.007 m, respectively.

Figure 12 shows the residual foundation rotations of the RC-SSI and SC-SSI frames under the DBE- and MCE-level excitations. The average residual foundation rotation of the RC-SSI frame is below the limit value of none damage under the DBEs. Under the MCEs, however, the average residual foundation rotation of the RC-SSI frame is 0.007 rad, exceeding the permissible limit of none damage. For the MCE hazard level, six ground motions cause the residual foundation rotations larger than the limit value of none damage, and one ground motion causes a residual foundation rotation greater than the limit value of light damage. In general, the residual foundation rotations of the SC-SSI frame are smaller than those of the RC-SSI frame. Under both the DBE- and MCE-level excitations, the residual foundation rotations of the SC-SSI frame are below the limit value of none damage at the mean level. However, there are four earthquake records of MCE hazard level that result in residual foundation rotations greater than 1/150 rad, indicating that the foundation system suffers slight damage.

7. Summary and Conclusions

This study evaluates the effect of SSI on the performance of self-centering (SC) concrete frames under the DBE- and

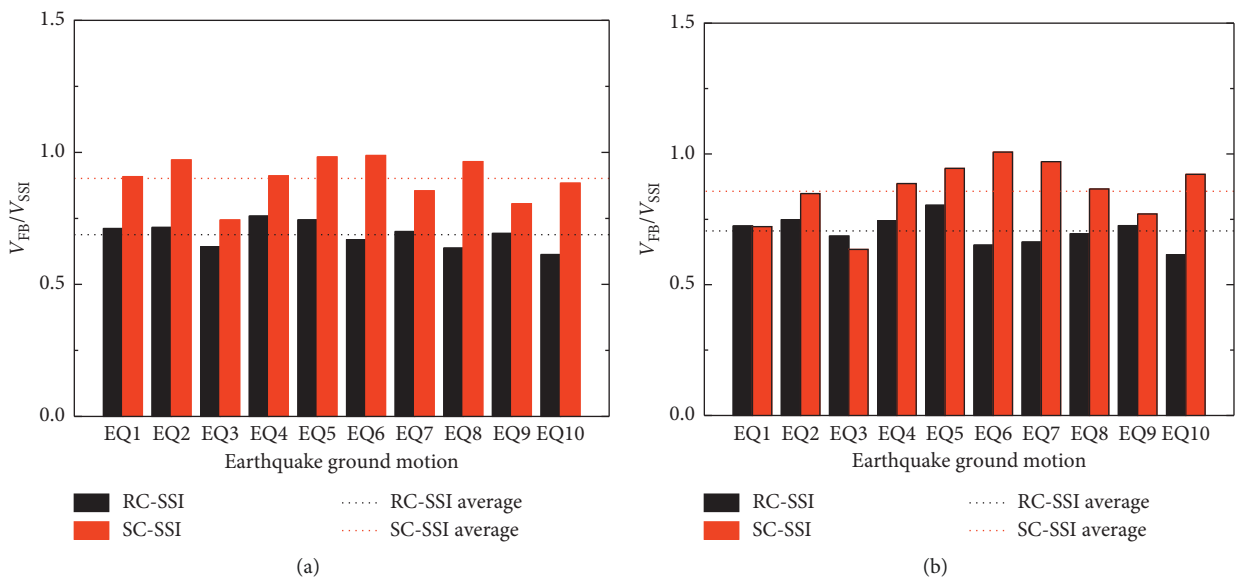

Figure 10: Base shear of the RC and SC frames with flexible foundations. (a) DBE. (b) MCE.

Table 3: Damage classification criteria of foundations [41].

Foundation tilting θ_t (rad)	Settlement S (m)			
	$S \le 0.05$	$0.05 < S \le 0.1$	$0.1 < S \le 0.3$	$S > 0.3$
$\theta_t \le 1/150$	None	Light	—	—
$1/150 < \theta_t \le 1/75$	Light	Moderate	Moderate	—
$1/75 < \theta_t \le 1/30$	Moderate	Moderate	Heavy	Heavy
$\theta_t > 1/30$	Heavy	Heavy	Heavy	Heavy

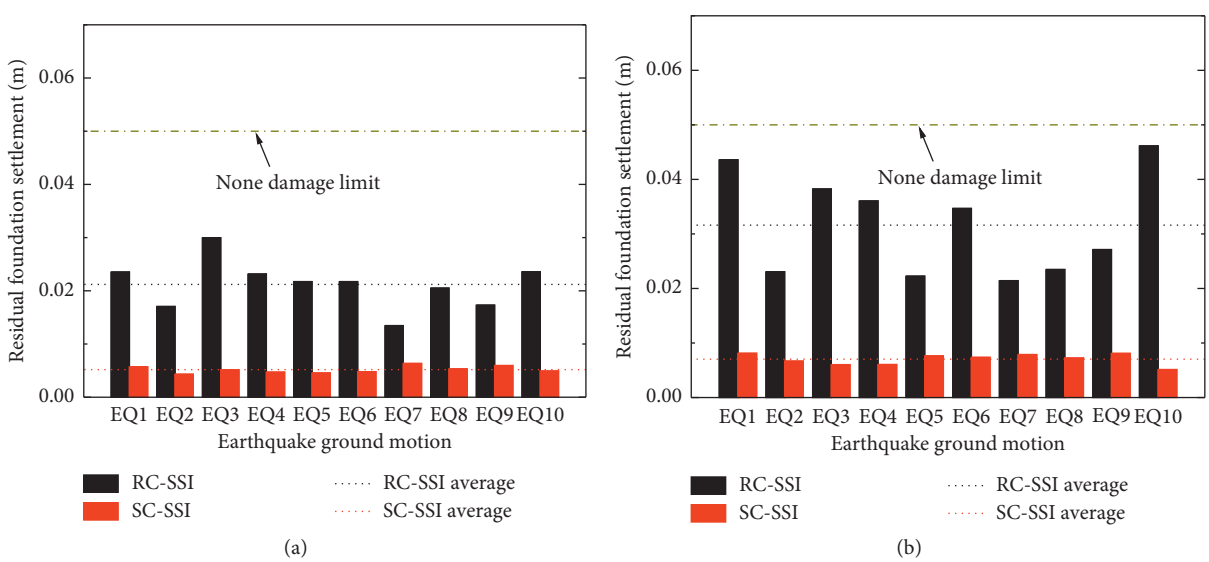

Figure 11: Residual foundation settlements of the RC-SSI and SC-SSI frames. (a) DBE. (b) MCE.

MCE-level excitations. Through the nonlinear dynamic analyses, the seismic responses of a set of 4-story SC and RC concrete frames, with and without flexible foundations, are comparatively investigated. According to the analysis results, the following conclusions can be summarized:

(1) Seismic analysis results show the SC and RC frames (with fixed and flexible base conditions) have similar peak story drift demands. Particularly, the SC-FB frame has slightly smaller maximum story drift demands than the RC-FB frame under the DBE- and

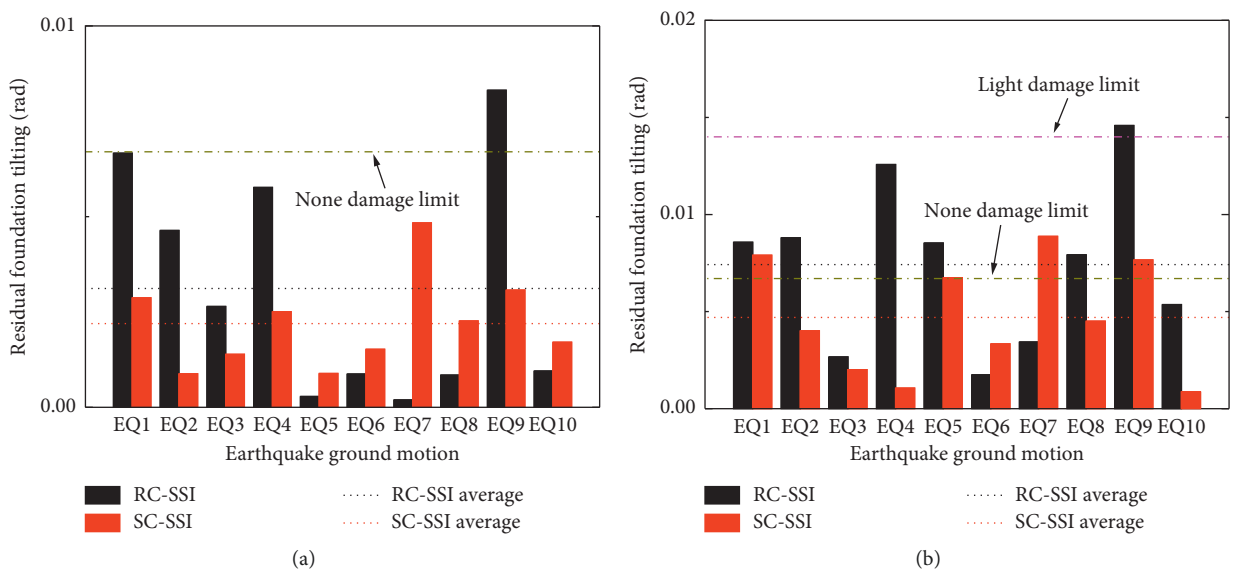

Figure 12: Residual foundation rotations of the RC-SSI and SC-SSI frames. (a) DBE. (b) MCE.

MCE-level excitations. When the SSI is considered, the peak story drift demands of the RC-SSI and SC-SSI frames are increased, and the SC-SSI frame has slightly larger peak story drift demands than the RC-SSI frame.

(2) Benefitting from their recentering capability, the SC frames experience significantly lower residual drift demands than the RC frames. Compared with their fixed base frame counterparts, the peak residual drift ratios of the RC-SSI frame are increased by 44.4% to 0.26% rad and by 35.6% to 0.61% rad at the DBE- and MCE-level excitations, respectively; and the peak residual drift ratios of the SC-SSI frame are increased by 27.3% to 0.14% rad and 10.3% to 0.32% rad at the DBE- and MCE-level excitations, respectively.

(3) Compared to their fixed base frame counterparts, the base shear demands of the RC-SSI and SC-SSI frames can reduce up to 30% and 10%, respectively, due to the SSI effect.

(4) When soil-structure interaction is considered, it is found that the connection of the SC-SSI frame sustains less rotation and dissipates less energy than the connection of the SC-FB frame.

(5) In general, the residual foundation deformations of the SC-SSI frame are smaller than those of the RC-SSI frame. The residual foundation settlements of both the RC-SSI and SC-SSI frames are within the permissible limit of none damage under all earthquake ground motions. On average, the residual foundation rotations of the SC-SSI frame are below the none damage limit value under the DBE- and MCE-level excitations, while the residual foundation rotation of the RC-SSI frame under the MCE is greater than the permissible limit of none damage.

It is worth noting that the conclusions drawn in this study are limited within the context of the chosen frames and foundations. Further investigations considering taller structures, different foundation, and soil types are required to get more generalized results for the self-centering prestressed concrete frames.

Data Availability

The data used to support the findings of this study are available from the corresponding author upon request.

Conflicts of Interest

The authors declare that they have no conflicts of interest regarding the publication of this paper.

Acknowledgments

The authors would like to acknowledge the support from the National Natural Science Foundation of China under Grant no. 51708172, the Natural Science Foundation of Jiangsu Province under Grant no. BK20170890, and the project funded by the China Postdoctoral Science Foundation under Grant no. 2019M651674.

References

[1] K. C. Tsai, C. P. Hsiao, and M. Bruneau, "Overview of building damages in 921 Chi-Chi earthquake," *Earthquake Engineering and Engineering Seismology*, vol. 2, no. 1, pp. 93–108, 2000.

[2] B. Zhao, F. Taucer, and T. Rossetto, "Field investigation on the performance of building structures during the 12 May 2008 Wenchuan earthquake in China," *Engineering Structures*, vol. 31, no. 8, pp. 1707–1723, 2009.

[3] J. M. Ricles, R. Sause, M. M. Garlock, and C. Zhao, "Post-tensioned seismic-resistant connections for steel frames," *Journal of Structural Engineering*, vol. 127, no. 2, pp. 113–121, 2001.

[4] C. Christopoulos, R. Tremblay, H.-J. Kim, and M. Lacerte, "Self-centering energy dissipative bracing system for the

seismic resistance of structures: development and validation," *Journal of Structural Engineering*, vol. 134, no. 1, pp. 96–107, 2008.

[5] C.-C. Chou and J.-H. Chen, "Seismic design and shake table tests of a steel post-tensioned self-centering moment frame with a slab accommodating frame expansion," *Earthquake Engineering & Structural Dynamics*, vol. 40, no. 11, pp. 1241–1261, 2011.

[6] P. M. Clayton, J. W. Berman, and L. N. Lowes, "Subassembly testing and modeling of self-centering steel plate shear walls," *Engineering Structures*, vol. 56, pp. 1848–1857, 2013.

[7] M. R. Eatherton, X. Ma, H. Krawinkler, G. G. Deierlein, and J. F. Hajjar, "Quasi-static cyclic behavior of controlled rocking steel frames," *Journal of Structural Engineering*, vol. 140, no. 11, Article ID 04014083, 2014.

[8] C.-X. Qiu and S. Zhu, "Performance-based seismic design of self-centering steel frames with SMA-based braces," *Engineering Structures*, vol. 130, pp. 67–82, 2017.

[9] M. A. Rahman and S. Sritharan, "Performance-based seismic evaluation of two five-story precast concrete hybrid frame buildings," *Journal of Structural Engineering*, vol. 133, no. 11, pp. 1489–1500, 2007.

[10] Y. C. Kurama, R. Sause, S. Pessiki, and L. W. Lu, "Lateral load behavior and seismic design of unbonded post-tensioned precast concrete walls," *ACI Structural Journal*, vol. 96, no. 4, pp. 625–632, 1999.

[11] M. J. N. Priestley and G. A. MacRae, "Seismic tests of precast beam-to-column joint subassemblages with unbonded tendons," *PCI Journal*, vol. 41, no. 1, pp. 64–81, 1996.

[12] W. C. Stone, G. S. Cheok, and J. F. Stanton, "Performance of hybrid moment-resisting precast beam-column concrete connection subjected to cyclic loading," *ACI Structural Journal*, vol. 92, no. 2, pp. 229–249, 1995.

[13] L. Li, J. B. Mander, and R. P. Dhakal, "Bidirectional cyclic loading experiment on a 3D beam-column joint designed for damage avoidance," *Journal of Structural Engineering*, vol. 134, no. 11, pp. 1733–1742, 2008.

[14] Y. Cui, X. Lu, and C. Jiang, "Experimental investigation of triaxial self-centering reinforced concrete frame structures through shaking table tests," *Engineering Structures*, vol. 132, pp. 684–694, 2017.

[15] B. G. Morgen and Y. C. Kurama, "A friction damper for post-tensioned precast concrete moment frames," *PCI Journal*, vol. 49, no. 4, pp. 112–133, 2004.

[16] L.-L. Song, T. Guo, and C. Chen, "Experimental and numerical study of a self-centering prestressed concrete moment resisting frame connection with bolted web friction devices," *Earthquake Engineering & Structural Dynamics*, vol. 43, no. 4, pp. 529–545, 2014.

[17] L.-L. Song, T. Guo, Y. Gu, and Z.-L. Cao, "Experimental study of a self-centering prestressed concrete frame subassembly," *Engineering Structures*, vol. 88, pp. 176–188, 2015.

[18] G. S. Cheok, W. C. Stone, and S. K. Kunnath, "Seismic response of precast concrete frames with hybrid connections," *ACI Structural Journal*, vol. 95, no. 5, pp. 527–539, 1998.

[19] B. G. Morgen and Y. C. Kurama, "Seismic response evaluation of posttensioned precast concrete frames with friction dampers," *Journal of Structural Engineering*, vol. 134, no. 1, pp. 132–145, 2008.

[20] L.-L. Song, T. Guo, and Z.-L. Cao, "Seismic response of self-centering prestressed concrete moment resisting frames with web friction devices," *Soil Dynamics and Earthquake Engineering*, vol. 71, pp. 151–162, 2015.

[21] J. P. Stewart, G. L. Fenves, and R. B. Seed, "Seismic soil-structure interaction in buildings. I: analytical methods," *Journal of Geotechnical and Geoenvironmental Engineering*, vol. 125, no. 1, pp. 26–37, 1999.

[22] J. P. Stewart, R. B. Seed, and G. L. Fenves, "Seismic soil-structure interaction in buildings. II: empirical findings," *Journal of Geotechnical and Geoenvironmental Engineering*, vol. 125, no. 1, pp. 38–48, 1999.

[23] S. C. Dutta, K. Bhattacharya, and R. Roy, "Response of low-rise buildings under seismic ground excitation incorporating soil-structure interaction," *Soil Dynamics and Earthquake Engineering*, vol. 24, no. 12, pp. 893–914, 2004.

[24] P. Raychowdhury, "Effect of soil parameter uncertainty on seismic demand of low-rise steel buildings on dense silty sand," *Soil Dynamics and Earthquake Engineering*, vol. 29, no. 10, pp. 1367–1378, 2009.

[25] G. Mylonakis and G. Gazetas, "Seismic soil-structure interaction: beneficial or detrimental?," *Journal of Earthquake Engineering*, vol. 4, no. 3, pp. 277–301, 2000.

[26] C. B. Haselton and G. G. Deierlein, "Assessing seismic collapse safety of modern reinforced concrete moment frame buildings," Report No. 156, John A. Blume Earthquake Engineering Center, Stanford University, California, CA, USA, 2007.

[27] International Code Council (ICC), *International Building Code*, Falls Church, Virginia, VA, USA, 2003.

[28] ASCE 7-02, *Minimum Design Loads for Buildings and Other Structure*, American Society of Civil Engineers, Reston, VA, USA, 2002.

[29] ACI 318-02, *Building Code Requirements for Reinforced Concrete*, American Concrete Institute Committee, Detroit, MI, USA, 2002.

[30] G. G. Meyerhof, "The ultimate bearing capacity of foudations," *Géotechnique*, vol. 2, no. 4, pp. 301–332, 1951.

[31] S. Mazzoni, F. McKenna, M. H. Scott, and G. L. Fenves, "OpenSees (open system for earthquake engineering simulation)," in *Pacific Earthquake Engineering Research (PEER) Center*, University of California, Berkeley, Berkeley, CA, USA, 2009.

[32] L. F. Ibarra, R. A. Medina, and H. Krawinkler, "Hysteretic models that incorporate strength and stiffness deterioration," *Earthquake Engineering & Structural Dynamics*, vol. 34, no. 12, pp. 1489–1511, 2005.

[33] C. B. Haselton, A. B. Liel, S. T. Lange, and G. G. Deierlein, "Beam-column element model calibrated for predicting flexural response leading to global collapse of RC frame buildings," Report No. 2007/03, Pacific Earthquake Engineering Research Center, University of California, Berkeley, Berkeley, CA, USA, 2007.

[34] H. Bobadilla and A. K. Chopra, "Evaluation of the MPA procedure for estimating seismic demands: RC-SMRF buildings," *Earthquake Spectra*, vol. 24, no. 4, pp. 827–845, 2008.

[35] M. Fragiadakis, D. Vamvatsikos, and M. Aschheim, "Application of nonlinear static procedures for the seismic assessment of regular RC moment frame buildings," *Earthquake Spectra*, vol. 30, no. 2, pp. 767–794, 2014.

[36] D. C. Kent and R. Park, "Flexural members with confined concrete," *Journal of the Structural Division*, vol. 97, no. 7, pp. 1969–1990, 1971.

[37] C. W. Harden and T. C. Hutchinson, "Beam-on-nonlinear-Winkler-foundation modeling of shallow, rocking-dominated footings," *Earthquake Spectra*, vol. 25, no. 2, pp. 277–300, 2009.

[38] R. W. Boulanger, C. J. Curras, B. L. Kutter, D. W. Wilson, and A. Abghari, "Seismic soil-pile-structure interaction experiments and analyses," *Journal of Geotechnical and Geoenvironmental Engineering*, vol. 125, no. 9, pp. 750–759, 1999.

[39] P. Raychowdhury and T. C. Hutchinson, "Performance evaluation of a nonlinear Winkler-based shallow foundation model using centrifuge test results," *Earthquake Engineering & Structural Dynamics*, vol. 38, no. 5, pp. 679–698, 2009.

[40] ATC-40, *Seismic Evaluation and Retrofit of Concrete Buildings*, Applied Technology Council (ATC), Redwood City, CA, USA, 1996.

[41] Y. Nakano, M. Maeda, H. Kuramoto, and M. Murakami, "Guideline for post-earthquake damage evaluation and rehabilitation of RC buildings in Japan," in *Proceedings of 13th World Conference on Earthquake Engineering*, Vancouver, Canada, August 2004.

[42] P. Raychowdhury, *Nonlinear Winkler-based shallow foundation model for performance assessment of seismically loaded structures*, Ph.D. thesis, University of California, San Diego, San Diego, CA, USA, 2008.